Table 2 Primary antibodies

Antibody	Species (clone)	Dilution	Source
Arterial cellular components			
von Willebrand factor	Rabbit	1:50	Ylem SRL
α-smooth muscle actin	Mouse (1A4)	1:100	Dako
Smooth muscle myosin heavy chain (SM1 & SM2)	Mouse (MAB3568)	1:100	Chemicon
CD68	Mouse (KP1)	1:100	Dako
Arterial non-cellular components			
Type I collagen	Mouse (I-8H5)	10 μg/mL	DFK
Type III collagen	Rabbit	1:500	LSL
Type IV collagen	Mouse (PHM-12)	prediluted	Ventana
Type IV collagen	Mouse (CIV22)	1:25	Dako
Type V collagen	Mouse (V-3C9)	10 μg/mL	DFK
Type VI collagen	Mouse (VI-26)	10 μg/mL	DFK
Type VIII collagen	Rabbit	1:50	LSL
Fibronectin	Mouse (TV-1)	2 μg/mL	Chemicon

evaluated for all the arteries in the leptomeninges, cortical gray matter, and white matter of each section.

Immunohistochemistry

Immunohistochemical investigations were performed using 6 μm-thick sections according to the standard biotin-streptavidin complex method. To perform the immunohistochemical reactions under specific conditions, a Ventana automated immunohistochemistry system (NexES, ver. 9.0; Ventana Medical Systems, Tucson, AZ, USA) was employed, and the Ventana DAB universal detection kit or the Ventana enhanced alkaline phosphatase red detection kit were utilized for the peroxidase-DAB method or the alkaline phosphatase-Fast Red method, respectively, according to the manufacturer's instructions. A battery of primary antibodies was employed to identify various components of the arterial walls (Table 2). For each antibody, sections were pretreated with an appropriate antigen retrieval method, microwave oven heating and/or enzyme digestion (pepsin, trypsin, or proteinase K). The sections were counterstained with hematoxylin. Additionally, for α-actin-immunohistochemistry, some sections were prestained using Weigert's method (resorcin and fuchsin) to visualize the elastic lamina. This double staining technique was used to identify the precise location of the SMCs, by depicting the basic laminar structure of vascular wall together with the immunohistochemical color development.

Electron microscopy

Leptomeningeal arteries with a caliber >1000 μm were dissected from formalin-fixed, paraffin-embedded tissue blocks of the frontal lobes from patients with CARASIL (patient 2), CADASIL, arteriosclerosis, or non-vascular diseases. The tissues were then deparaffinized and embedded in epoxy resin. Ultrathin sections were stained with uranyl acetate and lead citrate and examined under a JEM-1200EX II electron microscope (JEOL, Tokyo, Japan).

RESULTS

Conventional histochemistry

In both CARASIL cases, diffuse myelin pallor in the cerebral white matter with relative preservation of the U-fibers was confirmed (Fig. 1A). As to the cerebrovasculature, intimal proliferation, splitting of the internal elastic lamina, and occasional mural hyalinosis were found in small arteries with a diameter of 100–500 μm. Larger leptomeningeal arteries, including those with a diameter of more than 1000 μm also showed mild intimal proliferation (Fig. 1B). Elastica van Gieson staining clearly demonstrated that the internal elastic lamina was undulated and/or multilayered in many arteries (Fig. 1C). Double-barreling of the arterial wall was also frequent (Fig. 1D). In addition to these known pathologic findings, we also noticed that the affected arteries showed an obvious thinning of the media and adventitia, and most of the arteries appeared to be centrifugally enlarged especially in the leptomeninges and cerebral white matter (Fig. 1B–D). Actually, even in arteries without any intimal changes, the tunica media and adventitia appeared to be thinner than those in the CADASIL and other control cases (Fig. 1E–G). However, intense arteriosclerosis showing luminal narrowing was less frequent than had generally been supposed. In fact, small arteries showing wall thickening with narrowing of the lumen were mainly scattered in the basal ganglia; however, arteries with this type of change were scarcely found in leptomeninges and cortical parenchyma.

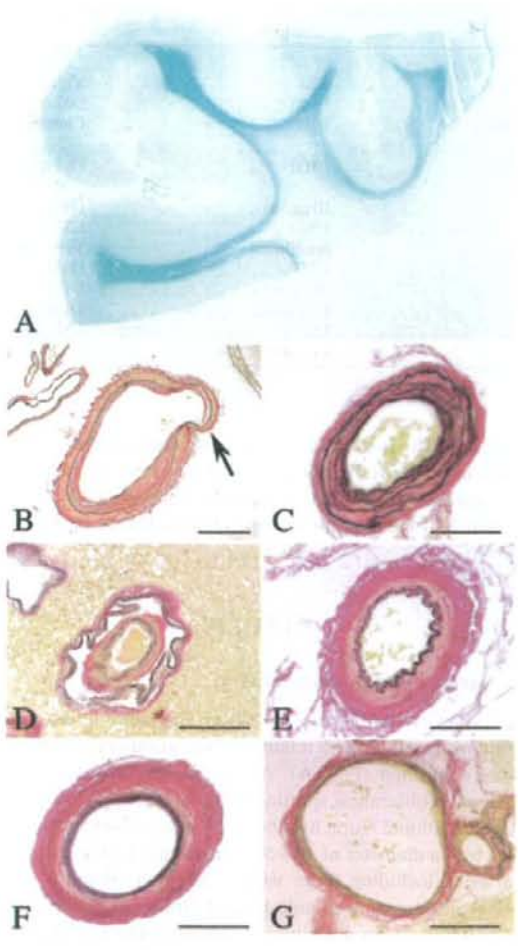

Fig. 1 Neuropathologic findings of cerebral autosomal recessive arteriopathy with subcortical infarcts and leukoencephalopathy (CARASIL). (A) Diffuse myelin pallor with preserved U-fibers in frontal cortex, CARASIL case 1. (B) Large leptomeningeal artery showing moderate intimal proliferation. Medial and adventitial thinning with aneurysmal formation is also seen (arrow). CARASIL case 1. (C) Leptomeningeal artery showing intimal proliferation and splitting of the internal elastic lamina. The media and adventitia are very thin. CARASIL, case 2. (D) Small artery in the cerebral white matter showing a markedly undulated internal elastic lamina. The arterial wall exhibits so-called "double-barreling". The medial tissue is almost completely lost and the outer rim of the internal elastic lamina appears to be in direct contact with the adventitia. CARASIL, case 1. (E) Leptomeningeal artery of nonarteriosclerotic control case. The wavy appearance of the internal elastic lamina is a normally occurring artifact caused by the contraction of medial smooth muscle cells (SMCs) at the time of tissue fixation. (F) Leptomeningeal artery of cerebral autosomal dominant arteriopathy with subcortical infarcts and leukoencephalopathy (CADASIL) case. The wavy appearance of the internal elastic lamina is not visible, reflecting the degeneration of the medial SMCs. However, the basic vascular structure is relatively preserved. (G) Leptomeningeal artery of CARASIL. This artery shows no intimal proliferation, but the tunica media and adventitia are appreciably thin and the lumen appears to be centrifugally enlarged. The internal elastic lamina is discontinuous. CARASIL case 1. A, Klüver-Barrera stain; B–G, elastica van Gieson stain. Bar in B indicates 500 μm. Bars in C–G indicate 100 μm.

SIs

Table 3 shows SI in frontal white matter and in leptomeningeal arteries.

In the white matter arteries, SIs of both CARASIL 1 (mean ± SD; 0.39 ± 0.14) and CARASIL 2 (0.25 ± 0.06) were smaller than SI of CADASIL (0.61 ± 0.13) ($P < 0.01$). There were no differences between SIs of CARASILs and SIs of nonarteriosclerotic controls, except for SI of CARASIL 1 (0.39 ± 0.14) over SI of nonarteriosclerotic control 1 (0.17 ± 0.06) ($P < 0.01$). SIs of CADASIL (0.61 ± 0.13) was larger than SIs of nonarteriosclerotic controls (0.17 ± 0.06 and 0.28 ± 0.07) ($P < 0.01$).

In the leptomeningeal arteries, SI of CARASIL 1 (0.31 ± 0.09) was smaller than CARASIL 2 (0.40 ± 0.10) ($P < 0.05$) and CADASIL (0.48 ± 0.12) ($P < 0.01$), but not different from SIs of nonarteriosclerotic controls. No difference was found in SIs of CARASIL 2 and SIs of CADASIL, arteriosclerotic control having subcortical infarcts (0.34 ± 0.12), or nonarteriosclerotic controls (0.36 ± 0.11, 0.32 ± 0.11) ($P < 0.01$).

Frequency of cerebral arterial changes

Our analysis revealed that medial and adventitial thinning with medial SMC loss was the most frequent pathologic finding in both CARASIL cases (Fig. 2). On the other hand, intimal proliferation and disruption of the internal elastic lamina were less frequent, and the frequency of these findings was higher in patient 2 than in patient 1. This difference might reflect the survival period of the two patients. These results indicate that the medial and adventitial changes are the primary pathologies and that these changes precede the intimal changes. Despite intimal proliferation, complete occlusion of the arterial lumen was actually rare. Conversely, most arteries were rather dilated, especially those located in the leptomeninges and subcortical white matter. The arterial dilatation was most likely due to the depletion of medial SMCs and the reduction in adventitial and medial interstitial connective tissue. These results prompted us to focus our immunohistochemical investigations on the medial SMCs and various components of the mural extracellular matrix (ECM).

Table 3 Sclerotic index (SI) of frontal white matter arteries (a) and leptomeningeal arteries (b) 50–200 μm in external diameter

Patients, age/sex	Sclerotic index (SI), mean ± SD (n = number of arteries)	Result of statistical analysis using Kuruskal Wallis test					
		CARASIL 1	CARASIL 2	CADASIL	Arteriosclerotic control having subcortical infarcts	Non-arteriosclerotic control 1	Non-arteriosclerotic control 2
(a) White matter arteries							
CARASIL 1, 35/M	0.39 ± 0.14 (n = 31)	/	n.s.	**	n.s.	**	n.s.
CARASIL 2, 51/F	0.25 ± 0.06 (n = 13)		/	**	n.s.	n.s.	n.s.
CADASIL, 75/M	0.61 ± 0.13 (n = 40)			/	n.s.	**	**
Arteriosclerotic control having subcortical infarcts, 70/F	0.44 ± 0.12 (n = 29)				/	**	n.s.
Non-arteriosclerotic control 1, 51/F	0.17 ± 0.06 (n = 19)					/	n.s.
Non-arteriosclerotic control 2, 61/F	0.28 ± 0.07 (n = 17)						/
(b) Leptomeningeal arteries							
CARASIL 1, 35/M	0.31 ± 0.09 (n = 57)	/	*	**	n.s.	n.s.	n.s.
CARASIL 2, 51/F	0.40 ± 0.10 (n = 39)		/	n.s.	n.s.	n.s.	n.s.
CADASIL, 75/M	0.48 ± 0.12 (n = 46)			/	**	**	**
Arteriosclerotic control having subcortical infarcts, 70/F	0.34 ± 0.12 (n = 71)				/	n.s.	n.s.
Non-arteriosclerotic control 1, 51/F	0.36 ± 0.11 (n = 69)					/	n.s.
Non-arteriosclerotic control 2, 61/F	0.32 ± 0.11 (n = 18)						/

*P < 0.05, **P < 0.01 using Kuruskal-Wallis test; n.s. not significant; CARASIL, cerebral autosomal recessive arteriopathy with subcortical infarcts and leukoencephalopathy; CADASIL, cerebral autosomal dominant arteriopathy with subcortical infarcts and leukoencephalopathy.

Immunohistochemistry

Arterial cellular components

Weigert and α-actin double staining clearly demonstrated that α-actin-immunolabeled medial SMCs were markedly reduced in all the CNS arteries in the CARASIL patients. Especially in arteries with a diameter of <500 μm, medial SMCs immunolabeled with the anti-α-actin antibody were almost completely lost. Of particular note, the media showed a weak or no immunoreactivity for anti-α-actin antibody even in almost normal-looking arteries without any intimal changes visible using conventional histopathological methods (Fig. 3A–D). In the thickened intima, α-actin-immunoreactive cells were often scattered in a random fashion, representing so-called "myointimal cells". In the CARASIL tissues, large leptomeningeal arteries with a diameter of more than 1000 μm showed only scattered α-actin-immunoreactive SMCs in the media, but the intensity of the immunostaining was much weaker than the intensities of the nonarteriosclerotic and arteriosclerotic control cases and weaker than that of the CADASIL case (Fig. 3E–H). Smooth muscle myosin heavy chain (SM1 and SM2)-immunohistochemistry revealed results similar to those for α-actin-immunohistochemistry (not illustrated).

Endothelial cells exhibiting von Willebrand factor-immunoreactivity were well preserved in all cases, including the CARASIL tissues. CD68-expressing foamy macrophages were frequently aggregated within the atheromas in the thickened intima of the vascular control cases. In contrast, CD68-positive cells were scarce, and those with a foamy form were never found in the arterial walls of CARASIL cases, indicating that monocyte/macrophage-lineage cells were less involved in the intimal lesion (not illustrated).

Arterial ECM

In vascular and non-vascular control cases, strong immunoreactivities for antitype I, III and VI collagen antibodies were observed in the adventitia and, to a lesser degree, the interstitium of the media surrounding SMCs (Fig. 4A,D). In the CADASIL case, the immunoreactivities for those collagen species were largely preserved or increased in the media and adventitia (Fig. 4B,E). In the CARASIL arteries, on the other hand, the immunoreactivities for antitype I, III and VI collagen antibodies were weak in the media and adventitia (Fig. 4C,F). Pia mater and dura mater exhibited immunoreactivities for antitype I, III and VI collagen

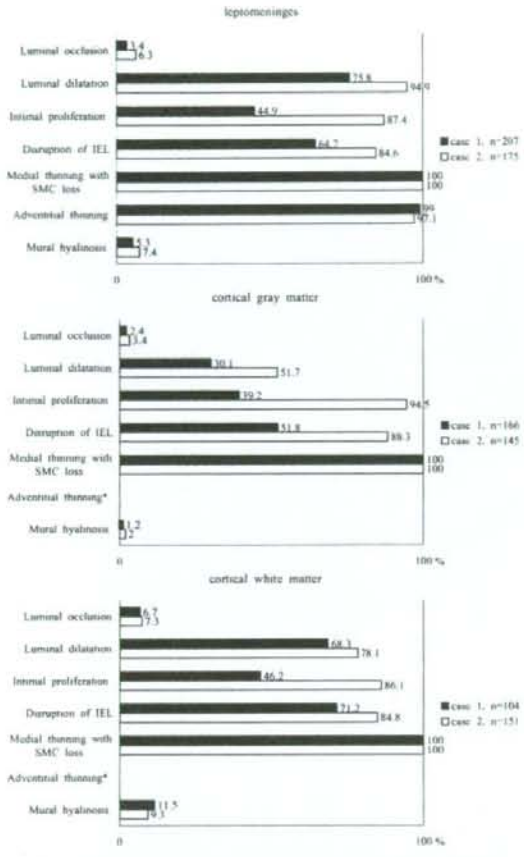

Fig. 2 Frequency of representative pathologic findings of cerebral autosomal recessive arteriopathy with subcortical infarcts and leukoencephalopathy (CARASIL) arteries. IEL, internal elastic lamina; SMC, smooth muscle cell. *Thinning of adventitia was not evaluated in parenchymal arteries, because adventitia of parenchymal arteries is usually very thin in control brains.

antibodies in the CARASIL cases, the same as the control cases (not illustrated). Fibronectin-immunoreactivity was colocalized with type I, III and VI collagen-immunoreactivities in all cases (Fig. 4G–I). In the nonarteriosclerotic control cases, type IV collagen-immunoreactivity was observed beneath the endothelial cells and in the media (Fig. 4J). In the arteriosclerotic control cases, the thickened intima often exhibited increased type IV collagen-immunoreactivity (not illustrated). On the other hand, type IV collagen-immunoreactivity was significantly reduced in the CADASIL and CARASIL cases, corresponding to the marked SMC loss, that is, a few surviving medial SMCs exhibited pericellular type IV collagen-immunoreactivity (Fig. 4K,L). Immunohistochemical staining for antitype V and VIII collagens was negative in all the cases.

Electron microscopy

Collagen fibrils with a diameter of 50–60 nm and characteristic cross-striations were identified in the extracellular space of the media and adventitia in the leptomeningeal arteries of the CARASIL patient (not illustrated). Bundles of collagen fibers were found in the vicinity of the fibroblasts in the adventitia. The ultrastructural findings of collagen fibrils in leptomeningeal arteries of the CARASIL case were the same as those in CADASIL, arteriosclerotic, and nonarteriosclerotic control cases.

DISCUSSION

To date, so-called "arteriosclerotic changes", fibrous intimal proliferation, splitting of the internal elastic lamina, and occasional hyaline degeneration of the wall have been reported as characteristic pathologic findings of CARASIL, and the resulting luminal stenosis has been believed to cause leukoencephalopathy. However, in the present study on two autopsied CARASIL brains, occluded arteries were observed infrequently. We evaluated intensity of small arterial sclerotic changes by the values of SI. In the literature SI values were reported as 0.2–0.3 in normal vessels, 0.3–0.5 in moderate small vessel diseases, and more than 0.5 in severe small vessel diseases.[10] In 51–70-years-old Japanese control patients, values of SIs in frontal medullary arteries were reported as 0.34–0.35.[11] In our study on frontal white matter arteries 50–200 μm in caliber, mean SIs of two nonarteriosclerotic controls were 0.17 and 0.28, which were in good agreement with those in previous reports.[10,11] In the white matter arteries, SIs of two CARASIL patients (0.39, 0.25) were significantly smaller than SI of CADASIL (0.61). There was no significant difference between SIs of CARASILs and nonarteriosclerotic controls, except for SI of CARASIL 1 over SI of nonarteriosclerotic control 1 in the frontal white matter arteries. In the leptomeningeal arteries, SI of CADASIL was significantly larger than SIs of nonarteriosclerotic controls, whereas no difference was found in SIs of CARASILs and nonarteriosclerotic controls. So far as SI is concerned, we conclude that the intensity of obliterative sclerotic changes of cerebral small arteries is mild in CARASIL as compared with CADASIL.

On the other hand, the present study demonstrated severe and widespread loss of arterial medial SMCs in CARASIL brains. Although a reduction in α-actin-immunolabeled SMCs in the arterial walls of CARASIL

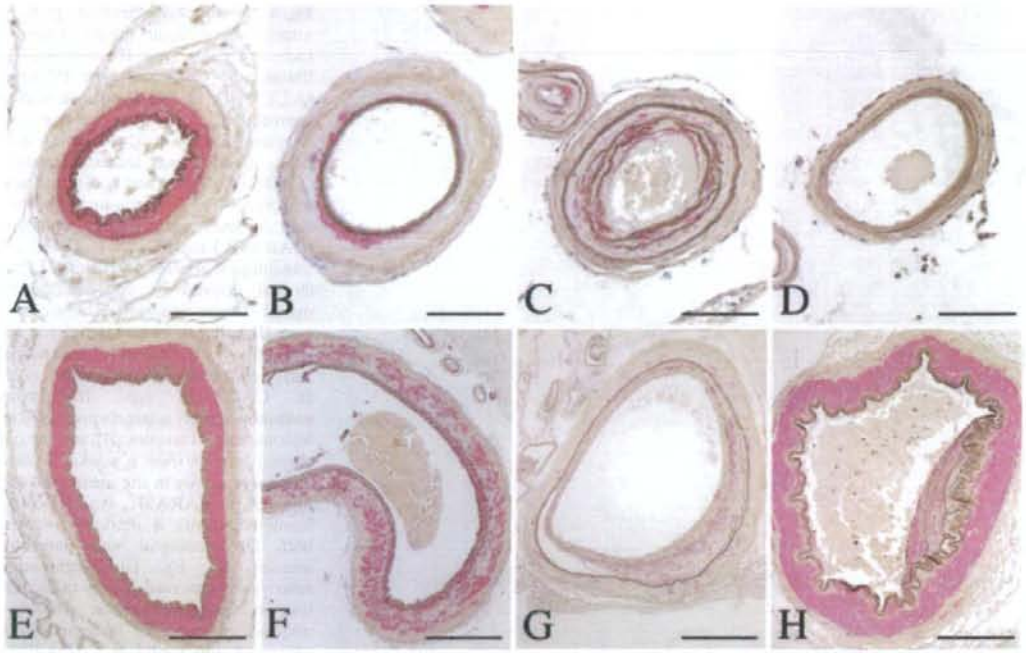

Fig. 3 Weigert and α-actin double staining. A–D Leptomeningeal small arteries with a diameter of 200 μm; E–H, leptomeningeal arteries with a diameter of 1000 μm. A and E, nonarteriosclerotic control; B and F, cerebral autosomal dominant arteriopathy with subcortical infarcts and leukoencephalopathy (CADASIL); C, D and G, cerebral autosomal recessive arteriopathy with subcortical infarcts and leukoencephalopathy (CARASIL) (case 2); H, arteriosclerotic control. In CADASIL, α-actin-positive medial smooth muscle cells (SMCs) are reduced, markedly in small-sized arteries (B) and moderately in large-sized arteries (F). In CARASIL, medial SMCs are almost completely lost in small-sized arteries (C), even in those without intimal proliferation (D). A few α-actin-positive cells scattered in the thickened intima represent so-called "myointimal cells" (C). Even in large arteries, the medial SMC loss is much more intense in CARASIL tissue (G) than in CADASIL tissue (F). The medial degeneration of the CARASIL arteries apparently differs from usual atherosclerosis, in which the medial SMCs are largely preserved (H). Bars in A–D indicate 100 μm. Bars in E–H indicate 500 μm.

tissues has been previously reported,[2] our Weigert and α-actin-double staining disclosed for the first time that α-actin-positive cells were almost completely lost from the media and that the vast majority of them were located in the thickened intima representing "myointimal cells". Furthermore, the medial thinning and SMC loss were more conspicuous than the sclerotic intimal changes. Actually, many arteries, especially those in the leptomeninges, did not exhibit sclerotic changes, while the medial SMCs were almost completely lost. We therefore believe that the medial SMC layer may be the primary site responsible for the pathophysiology of CARASIL, and this salient feature also clearly distinguishes CARASIL from usual arteriosclerosis and atherosclerosis. In CADASIL, medial SMC loss may deprive the cerebral arteries of their ability to regulate blood flow, leading to leukoencephalopathy.[12,13] Recent studies on Binswanger's disease also demonstrated that medial SMC loss, rather than luminal stenosis or adventitial fibrosis, was the principal factor causing diffuse myelin loss.[14,15] The same mechanism has been implicated in the pathogenesis of amyloid angiopathy-related leukoencephalopathy, in which amyloid-bearing arteries exhibit medial thinning with SMC loss.[16] This line of evidence suggests that the autoregulation of cerebral blood flow is severely affected in CARASIL because of the reduced contractile capacity caused by the medial SMC wasting. In addition, despite the limitation of the small number of cases examined in this study, the extent of medial SMC loss in CARASIL appears to be more than equal to that in CADASIL, especially in the large (proximal) leptomeningeal arteries. This pathologic finding might cause the neuroradiological differences between CARASIL and CADASIL; in the former the leukoencephalopathy is more diffuse and homogenous. The different prognoses of these two diseases may also be based on essential differences in vascular pathology.

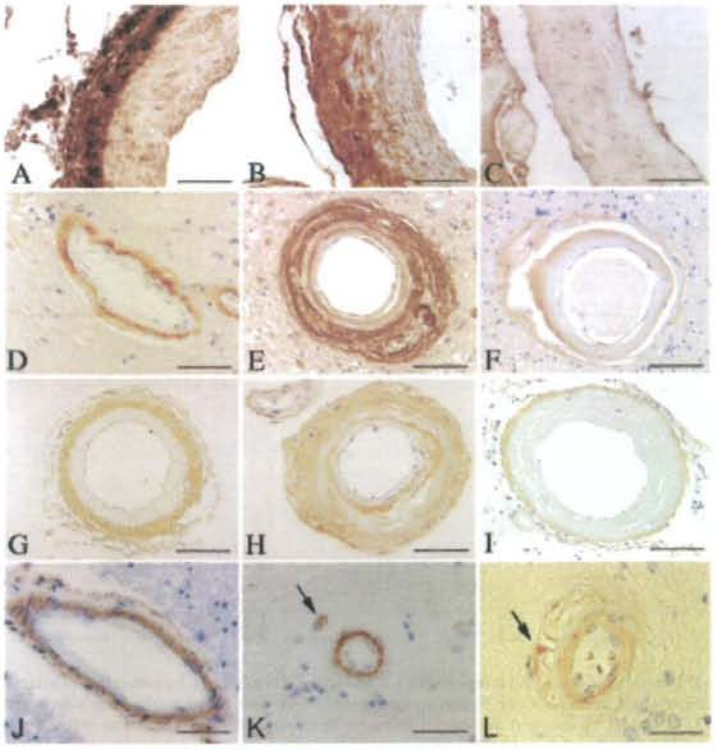

Fig. 4 Immunohistochemical profiles of arterial extracellular matrix. Immunohistochemistry for type III collagen (A–F), fibronectin (G–I), and type IV collagen (J–L). A, D, G and J, nonarteriosclerotic control; B, E, H and K, cerebral autosomal dominant arteriopathy with subcortical infarcts and leukoencephalopathy (CADASIL); C, F, I and L, cerebral autosomal recessive arteriopathy with subcortical infarcts and leukoencephalopathy (CARASIL) (case 2). A–C and G–I, leptomeningeal arteries; D–F and J–L, parenchymal arteries in the cerebral white matter. In the nonarteriosclerotic control, type III collagen-imunoreactivity is strong and diffuse in the adventitia and moderate and pericellular in the media (A, D). In CADASIL, type III collagen-immunoreactivity is largely preserved in the leptomeningeal arteries (B), and the parenchymal arteries show a markedly stronger immunoreactivity in the media and adventitia (E). In CARASIL, type III collagen-immunoreactivity is markedly weaker in both leptomeningeal and parenchymal arteries (C, F). Fibronectin-immunoreactivity is observed mainly in the adventitia in nonarteriosclerotic control (G), whereas, is markedly increased in both adventitia and media in CADASIL (H). Markedly decreased fibronectin-immunoreactivity is evident in the thinned adventitia in CARASIL tissue (I). In the nonarteriosclerotic control, type IV collagen-immunoreactivity is observed beneath the endothelial cells and around the medial smooth muscle cells (SMCs) (J). Type IV collagen-immunoreactivity is decreased in both CADASIL (K) and CARASIL (L), in which the staining is almost restricted beneath the endothelial cells. In the media, a few surviving SMCs exhibit pericellular immunostaining (arrows in K and L). Bars in A–I indicate 100 μm. Bars in J–L indicate 50 μm.

The other notable finding in this study was that the adventitia of the CARASIL arteries was appreciably thinner than those of the control cases, including the CADASIL tissues. This adventitial change may aggravate the fragility of the arterial walls, resulting in splitting, elongation, and the undulation of the internal elastic lamina leading to the double-barreling of the wall and finally the collapse of the arterial structure. We thus propose that the centrifugal enlargement of the arterial caliber caused by medial and adventitial degeneration precedes the centripetal intimal proliferation, the latter phenomenon reflecting a compensative remodeling for the tensile force on the disrupted walls. Because SMCs are known to produce the ECM including collagens,[17] whether the paucity of mural ECM is the cause or the result of medial SMC loss remains to be elucidated. Reduction of type IV collagen-immunoreactivity was observed in both CARASIL and CADASIL patients. This suggests that basement membrane-related type IV collagen is non-specifically decreased due to the medial SMC loss. On the other hand, immunoreactivities of type I, III and VI collagens and fibronectin were specifically decreased in CARASIL. It is also of note that other vasculopathic encephalopathies with medial SMC loss, like Binswanger's disease and CADASIL, exhibit medial and/or adventitial fibrosis with increased immunoreactivities for certain collagens,[18–21] suggesting that SMC loss does not necessarily cause ECM reduction. Therefore, we speculate that the ECM abnormality is upstream of the SMC degeneration in the pathogenesis of CARASIL. Existence of the characteristic dermato-osteo-arthropathy of CARASIL also indicates the possibility of underlying systemic disorder of the ECM. It is well known that alterations in the major collagen species and related proteins cause combined dermato-skeletal and vascular disorders, as in Ehlers–Danlos syndrome, Marfan's syndrome, and osteogenesis imperfecta.[22] Nowadays, it is widely accepted that the medial SMCs change their phenotype from a differentiated (contractile) to a dedifferentiated (synthetic) form, and vice versa, depending on the local environmental signal.[23–25] Especially, fibrillar collagens are known to be an

important signal for preserving the functional integrity of the contractile phenotype of arterial medial SMCs.[26,27] Interestingly, a previous study on biopsied skin from a patient with CARASIL demonstrated that skin pathology of CARASIL resembled that of lipoid proteinosis, an autosomal recessive disorder recently found to be caused by mutations in the extracellular matrix protein 1 (ECM1) gene, which is known to regulate endochondral bone formation and angiogenesis.[28-30] In CARASIL therefore, we can infer that some abnormalities in the mural ECM cause medial SMC alterations by the absence of its proper interaction with the SMCs. It is not likely that the major collagen species are primarily affected in CARASIL, because immunoreactivities for type I, III and VI collagens were preserved in pia mater and dura mater, and ultrastructural findings of collagen fibrils in the CARASIL case were not different from those in control cases. We suspect that some structural proteins or proteins interacting with the arterial mural ECM may be likely candidates for the pathogenesis of CARASIL.

Altogether, the extensive loss of medial SMCs and mural ECM deprives the cerebrovasculature of its structural and functional ability to regulate cerebral blood flow and is therefore critically involved in the development of diffuse leukoencephalopathy in CARASIL.

ACKNOWLEDGMENTS

We would like to thank Mss. A. Sakamoto and N. Kosugi, Department of Laboratory Medicine, Musashi Hospital, National Center of Neurology and Psychiatry, for their excellent technical assistance. Control brain samples were obtained from Research Resource Network for Brain Tissue, Japan. This study was supported by Grants from Ministry of Health, Labour and Welfare, Japan.

REFERENCES

1. Yanagawa S, Ito N, Arima K, Ikeda S. Cerebral autosomal recessive arteriopathy with subcortical infarcts and leukoencephalopathy. *Neurology* 2002; **58**: 817–820.
2. Arima K, Yanagawa S, Ito N, Ikeda S. Cerebral arterial pathology of CADASIL and CARASIL (Maeda syndrome). *Neuropathology* 2003; **23**: 327–334.
3. Maeda S, Nakayama H, Isaka K, Aihara Y, Nemoto S. Familial unusual encephalopathy of Binswanger's type without hypertension. *Folia Psychiatr Neurol Jpn* 1976; **30**: 165–177.
4. Fukutake T, Hattori T, Kita K, Hirayama K. Familial juvenile encephalopathy (Binswanger type) with alopecia and lumbago – a syndrome. *Rinsho Shinkeigaku* 1985; **25**: 949–955.
5. Fukutake T, Hirayama K. Familial young-adult-onset arteriosclerotic leukoencephalopathy with alopecia and lumbago without arterial hypertension. *Eur Neurol* 1995; **35**: 69–79.
6. Bowler JV, Hachinski V. Progress in the genetics of cerebrovascular disease: inherited subcortical arteriopathies. *Stroke* 1994; **25**: 1696–1698.
7. Fukutake T. Young-adult-onset hereditary subcortical vascular dementia: cerebral autosomal recessive arteriosclerosis with subcortical infarcts and leukoencephalopathy (CARASIL). *Rinsho Shinkeigaku* 1999; **39**: 50–52.
8. Ruchoux MM, Maurage CA. CADASIL: cerebral autosomal dominant arteriopathy with subcortical infarcts and leukoencephalopathy. *J Neuropathol Exp Neurol* 1997; **56**: 947–964.
9. Nishio T, Arima K, Eto K, Ogawa M, Sunohara N. Cerebral autosomal dominant arteriopathy with subcortical infarcts and leukoencephalopathy – report of an autopsied Japanese case. *Rinsho Shinkeigaku* 1997; **37**: 910–916.
10. Lammie GA, Brannan F, Slattery J, Warlow C. Nonhypertensive cerebral small vessel disease. An autopsy study. *Stroke* 1997; **28**: 2222–2229.
11. Furuta A, Ishii N, Nishihara Y, Horie A. Medullary arteries in aging and dementia. *Stroke* 1991; **22**: 442–446.
12. Pfefferkorn T, von Stuckrad-Barre S, Herzog J, Gasser T, Hamann GF, Dichgans M. Reduced cerebrovascular CO_2 reactivity in CADASIL. A transcranial Doppler sonography study. *Stroke* 2001; **32**: 17–21.
13. Okeda R, Arima K, Kawai M. Arterial changes in cerebral autosomal dominant arteriopathy with subcortical infarcts and leukoencephalopathy (CADASIL) in relation to pathogenesis of diffuse myelin loss of cerebral white matter. Examination of cerebral medullary arteries by reconstruction of serial sections of an autopsy case. *Stroke* 2002; **33**: 2565–2569.
14. Tanoi Y, Okeda R, Budka H. Binswanger's encephalopathy: serial sections and morphometry of the cerebral arteries. *Acta Neuropathol (Berl)* 2000; **100**: 347–355.
15. Okeda R, Murayama S, Sawabe M, Kuroiwa T. Pathology of the cerebral artery in Binswanger's disease in the aged: observation by serial sections and morphometry of the cerebral arteries. *Neuropathology* 2004; **24**: 21–29.
16. Imaoka K, Kobayashi S, Fujihara S, Shimode K, Nagasaki M. Leukoencephalopathy with cerebral amyloid angiopathy: a semiquantitative and morphometric study. *J Neurol* 1999; **246**: 661–666.
17. Mayne R. Collagenous proteins of blood vessels. *Arteriosclerosis* 1986; **6**: 585–593.

18. Zhang WW, Olsson Y. The angiopathy of subcortical arteriosclerotic encephalopathy (Binswanger's disease): immunohistochemical studies using markers for components of extracellular matrix, smooth muscle actin and endothelial cells. *Acta Neuropathol (Berl)* 1997; **93**: 219–224.
19. Lin JX, Tomimoto H, Akiguchi I *et al.* Vascular cell components of the medullary arteries in Binswanger's disease brains. A morphometric and immunoelectron microscopic study. *Stroke* 2000; **31**: 1838–1842.
20. Kalimo H, Ruchoux MM, Viitanen M, Kalaria RN. CADASIL: a common form of hereditary arteriopathy causing brain infarcts and dementia. *Brain Pathol* 2002; **12**: 371–384.
21. Miao Q, Paloneva T, Tuominen S *et al.* Fibrosis and stenosis of the long penetrating cerebral arteries: the cause of the white matter pathology in cerebral autosomal dominant arteriopathy with subcortical infarcts and leukoencephalopathy. *Brain Pathol* 2004; **14**: 358–364.
22. Schievink WI, Michels VV, Piepgras DG. Neurovascular manifestations of heritable connective tissue disorders. A review. *Stroke* 1994; **25**: 889–903.
23. Owens GK. Regulation of differentiation of vascular smooth muscle cells. *Physiol Rev* 1995; **75**: 487–517.
24. Hedin U, Thyberg J, Roy J, Dumitrescu A, Tran PK. Role of tyrosine kinases in extracellular matrix-mediated modulation of arterial smooth muscle cell phenotype. *Arterioscler Thromb Vasc Biol* 1997; **17**: 1977–1984.
25. Ishii I, Tomizawa A, Kawachi H *et al.* Histological and functional analysis of vascular smooth muscle cells in a novel culture system with honeycomb-like structure. *Atherosclerosis* 2001; **158**: 377–384.
26. Koyama H, Raines EW, Bornfeldt KE, Roberts JM, Ross R. Fibrillar collagen inhibits arterial smooth muscle proliferation through regulation of Cdk2 inhibitors. *Cell* 1996; **87**: 1069–1078.
27. Ichii T, Koyama H, Tanaka S *et al.* Fibrillar collagen specifically regulates human vascular smooth muscle cell genes involved in cellular responses and the pericellular matrix environment. *Circ Res* 2001; **88**: 460–467.
28. Arisato T, Hokezu Y, Suehara M, Kiwaki S, Kuriyama M, Osame M. Juvenile Binswanger-type encephalopathy with alopecia and spondylosis deformans – A case report. *Rinsho Shinkeigaku* 1993; **33**: 400–404.
29. Hamada T, Mclean WH, Ramsay M *et al.* Lipoid proteinosis maps to 1q21 and is caused by mutations in the extracellular matrix protein 1 gene (ECM1). *Hum Mol Genet* 2002; **11**: 833–840.
30. Chan I. The role of extracellular matrix protein 1 in human skin. *Clin Exp Dermatol* 2004; **29**: 52–56.

17 was cloned. In the present study, 42 unrelated patients from the Washington University Alzheimer's Disease Research Center (WUADRC) with clinically diagnosed FTLD and/or neuropathologically characterized cases of FTLD-U with or without MND were screened for mutations in *PGRN*. Bidirectional sequencing was performed for mutational screening. Mechanistically, most mutations in *PGRN* described thus far have been reported to display a haploinsufficiency through nonsense mediated decay (NMD). We describe a novel missense mutation in exon 1 (c.4068 C>A) introducing a charged amino acid in the hydrophobic core of the signal peptide at residue 9 (A9D) which displayed no significant difference in the total postmortem brain *PGRN* mRNA between cases and controls. In SHSY-5Y neuroblastoma cells overexpressed with mutant or wild-type *PGRN*, subcellular fractionation, biochemistry, and confocal microscopy indicate that mutant protein is expressed, but is not processed, through the ER for secretion, and appears to be misslocalized in the cytosol possibly resulting in a functional haploinsufficiency. This defect in trafficking results in a decrease in cell viability: an alternative *in vitro* model of FTLD-U with *PGRN* mutation neurodegeneration. Support for this work was provided by grants from the National Institute on Aging of the National Institutes of Health (P01-AG03991, P50-AG05681) and the Buchanan Fund.

58.8

High specificity and sensitivity of olfactory bulb synucleinopathy for lewy body disorders

Thomas G. Beach[1], Charles L. White[2], Christa Hladik[2], Marwan N. Sabbagh[1], Donald J. Connor[1], John N. Caviness[3], Lucia I. Sue[1], Jeanne Sasse[1], Jyothi Bachalakuri[1], Haru Akiyama[4], Charles H. Adler[3]. [1]Sun Health Research Institute, Sun City, AZ, [2]Division of Neuropathology, University of Texas Southwestern, Dallas, TX, [3]Department of Neurology, Mayo Clinic Arizona, Scottsdale, AZ, [4]Tokyo Institute of Psychiatry, Tokyo, Japan

Recent reports have suggested a high prevalence of olfactory bulb synucleinopathy in Lewy body disorders but there have been no estimates of the sensitivity or specificity of this as a diagnostic test. We performed α-synuclein immunostaining on paraffin-embedded sections of olfactory bulb from a series of neuropathologically-diagnosed subjects from the Sun Health Research Institute Brain Donation Program/Arizona Parkinson's Disease Consortium. Included in the series were 76 normal elderly individuals, 8 subjects with incidental Lewy body disease (ILBD), 63 with Parkinson's disease (PD) and 79 with dementia with Lewy bodies (DLB). Sections were stained with a sensitive method employing pretreatment with proteinase K. The ratios of positive to negative olfactory bulb staining for each diagnostic category were: normal 5/71; ILBD 8/0; PD 57/6; DLB 74/5. An α-synuclein-positive olfactory bulb has 92% sensitivity and 93% specificity for the diagnosis of PD versus normal while for DLB it is 94% and 93%, respectively. As all 8 cases of ILBD had a positive olfactory bulb it appears that olfactory bulb synucleinopathy may also be a reliable marker of presymptomatic Lewy body disorders. Supported by the AZ Dept. of Health Services, NIA P30 AG19610 and the Prescott Family Initiative of the Michael J. Fox Foundation.

58.9

Expression of alpha-synuclein (AS) in autonomic neurons is increased in Parkinson's disease (PD)

David G. Munoz, Andrea Gold. Laboratory Medicine, St. Michael's Hospital, University of Toronto & Li Ka Shing Knowledge Institute, Toronto, Canada

Background and objective: We have previously shown that expression of the main protein constituent of Lewy bodies, AS, is detectable in autonomic neurons in a subset of the adult population. The objective was to determine whether expression has greater prevalence or intensity in PD than in the general population or patients with Alzheimer's disease (AD).

Methods: Archival autopsy samples of colon obtained from adult patients with pathologically confirmed PD, AD, or no neurological disease were immunostained with anti AS antibody KM51 diluted 1:70 and visualized with a MACH 3 polymer kit. The expression was scored as absent (AS-), or present (AS+) in perikarya or terminals, semiquantitevely rated 1 to 3.

Results: Just over ⅓ of 70 subjects with no neurological disease were AS+: neither prevalence nor intensity varied by age over 40 years. Differences between sexes were not significative (NS). All 10 PD patients were AS+ as compared to 25 of 54 age-matched subjects ($p < 0.002$). The average intensity was also significantly greater ($p < 0.002$). In contrast 3 of 8 AD cases were AS+ (NS as compared with normal population).

Conclusion: AS+ in autonomic neurons is common in the adult population. This trait is significantly more prevalent and intense in PD, but not in AD. Either the development of PD increases AS expression, or PD preferentially develops in AS+ subjects.

58.10

Alpha-synucleinopathy is associated with spinocerebellar ataxia type 2 with Parkinsonism

Masaki Takao[1], Yoshio Sakiyama[2], Yuko Saito[2], Masahiro Aoyama[1], Harumi Shiroyama[3], Hiroshi Kurisaki[3], Kinya Ishikawa[4], Kuniaki Tsuchiya[5], Ban Mihara[1], Shigeo Murayama[2]. [1]Intractable Neurology and Cognitive Disorders, Mihara Memorial Hospital, Isesaki, Gunma, Japan, [2]Tokyo Metropolitan Institute of Gerontology, Itabashi-ku, Tokyo, Japan, [3]Tokyo Hospital, Kiyose, Tokyo, Japan, [4]Tokyo Medical and Dental University, Tokyo, Japan, [5]Matsuzawa Hospital, Tokyo, Japan

Levodopa-responsive Parkinsonism may be dominant phenotype of patients with SCA2. In general, they have a shorter abnormal expansion of CAG repeats (less than 39) in *ATXN2* gene. The aim is to elucidate neuropathologic basis of this variant SCA2 from different Japanese families and give a new perspective on pathogenesis of SCA2 with Parkinsonism.

Case 1: He was diagnosed as having Parkinson's disease at age 50. At age 65, he showed cerebellar ataxia and slow eye movement.

Case 2: He developed unstable gait at age 40. In addition to the ataxia, he had rigidity, bradykinesia, stooped posture and freezing gait. Genetic analyses of *ATXN2* showed an expanded CAG repeat with 22/38 (case 1) and 22/37 (case 2).

Neuropathology: There is an atrophy of the pons and cerebellum. The most striking finding was the presence of α-synuclein immunoreactive Lewy bodies (LBs) and neuritis (LNs) in the locus coeruleus, dorsal motor nucleus of vagus, basal nucleus of Meynert and amygdala. LBs and LNs were also seen in the substantia nigra. The distribution of Lewy pathology was consistent with stage 2 (case 1) and stage 3 (case 2) according to Braak's criteria. The 1C2 antibody depicted intranuclear immunopositive deposits in the various regions. In addition, α-synuclein deposits were not seen in SCA2 cases without Parkinsonism.

We conclude that α-synucleinopathy is vital pathologic alterations of SCA2 with Parkinsonism. JSPS 19500311.

58.11

TGFb-HIPK2 Signaling Pathway in the Survival of Dopamine Neurons During Toxin-induced Degeneration

Jiasheng Zhang, Eric J. Huang. Pathology, University of California San Francisco, San Francisco, CA

The current study investigates TGFb-HIPK2 signaling pathway in MPTP-induced degeneration of DA neurons. Our results indicate that loss of HIPK2 leads to a near complete protection of DA neurons from MPTP-induced cell death. Whereas MPTP treatment induces a robust increase in c-jun phosphorylation after MPTP in *wild type* DA neurons, no phospho-c-jun is detected in the DA neurons of *Hipk2* mutants. To determine if HIPK2 is sufficient for MPTP-induced cell death, we used a genetic approach to selectively express additional copies of HIPK2 in DA neurons. Our results indicate that DA neurons in conditional mouse mutants expressing extra copies of HIPK2 show a dose-dependent increase in MPTP-induced cell loss. Taken together, these results support the notion that,

1D05　短期間の理学療法介入が筋萎縮性側索硬化症患者の呼吸機能に及ぼす影響

[1]脳血管研究所美原記念病院　リハビリテーション科，[2]脳血管研究所美原記念病院　神経内科，
[3]脳血管研究所美原記念病院　神経難病・認知症部門
菊地　豊[1]，藤本　幹雄[1]，門脇　太郎[2]，高尾　昌樹[3]，美原　盤[3]

【目的】筋萎縮性側索硬化症（ALS）に対する短期間の理学療法介入が呼吸機能に及ぼす影響を検討した．【方法】ELescorial改訂版にてdefiniteないしprobableに分類されたALS患者9名（年齢61.4±13.7歳，罹病期間27.8±16.0ヵ月ALS-FRS-R 36.1±7.7，BiPAP夜間装着2例，球麻痺症状4例，気管切開例なし）を対象とした．理学療法は2週間の入院期間中に1日1時間，計10日間実施した．理学療法プログラムには，患者の状態に合わせて呼吸理学療法，バランスエクササイズを理学療法士が実施した．理学療法実施前後でマイクロスパイロHI-201（日本光電）を用い，％肺活量（%VC），％努力性肺活量（%FVC），最大中間呼気流量（MMF），最大呼気流量（PEF）を計測した．統計学的検定にはWilcoxon符号付順位和検定を用いた．【結果】各指標の実施前後の結果は，%VC（実施前58.0±26.2%，実施後62.3±26.6%，p=0.03），%FVC（実施前47.6±24.9%，実施後51.8±24.5，p=0.12），MMF（実施前2.78±1.53*l*，実施後3.03±1.72*l*，p=0.16），PEF（実施前3.87±2.30*l*/s，実施後4.26±2.20*l*/s，p=0.09）であった．【結論】ALSに対する短期間の理学療法介入は胸郭コンプライアンスの改善に寄与している可能性が示唆された．

1D06　非侵襲的人工呼吸器の機種比較—臨床工学技士のアンケート調査より—

[1]東芝林間病院　神経内科，[2]北里大学医学部　神経内科学，[3]北里大学東病院
荻野　裕[1]，荻野美恵子[2]，瓜生　伸一[3]，坂井　文彦[2]

【目的】現在NPPVに使用されている複数の機種についてMEの立場から見たメリット，デメリットを明らかにする．【方法・対象】現在採用しているBiPAP Harmony，Synchrony，Harmony S/T，KnightStar 330，レジェンドエアについて臨床工学技士6名に操作性や使いやすさ計12項目について5段階評価のアンケートを実施した．【結果】設定の確認，変更のしやすさ，医療従事者以外の人の使いやすさでBiPAP Synchronyとレジェンドエアが高得点であった．KnightStar 330は設定の確認，変更のしやすさ，機械の作動の安定性，安全性管理で低得点であった．外観，作動音，アラーム，インターフェイス，管の接続では差異は少なかった．【考案】今回の調査ではBiPAP Synchronyとレジェンドエアが高評価であった．KnightStar 330はロック機構の煩雑さ，容易に設定が変わってしまうこと，バッテリー切り替え時の不安定さの指摘があり評価が低かった．

ORIGINAL ARTICLE

A New Amyloid β Variant Favoring Oligomerization in Alzheimer's-Type Dementia

Takami Tomiyama, PhD,[1] Tetsu Nagata, MD, PhD,[2] Hiroyuki Shimada, MD, PhD,[3] Rie Teraoka, BSc,[1] Akiko Fukushima, MSc,[1] Hyoue Kanemitsu, PhD,[1] Hiroshi Takuma, MD, PhD,[1] Ryozo Kuwano, MD, PhD,[4] Masaki Imagawa, MD, PhD,[5] Suzuka Ataka, MD,[6,7] Yasuhiro Wada, MSc,[6,7] Eito Yoshioka, PhD,[6,7] Tomoyuki Nishizaki, MD, PhD,[2] Yasuyoshi Watanabe, MD, PhD,[6,7] and Hiroshi Mori, PhD[1]

Objective: Soluble oligomers of amyloid β (Aβ), rather than amyloid fibrils, have been proposed to initiate synaptic and cognitive dysfunction in Alzheimer's disease (AD). However, there is no direct evidence in humans that this mechanism can cause AD. Here, we report a novel amyloid precursor protein *(APP)* mutation that may provide evidence to address this question.

Methods: A Japanese pedigree showing Alzheimer's-type dementia was examined for mutations in *APP, PSEN1,* and *PSEN2.* In addition, 5,310 Japanese people, including 2,121 patients with AD, were screened for the novel *APP* mutation. The pathogenic effects of this mutation on Aβ production, degradation, aggregation, and synaptotoxicity were also investigated.

Results: We identified a novel *APP* mutation (E693Δ) producing variant Aβ lacking gulutamate-22 (E22Δ) in Japanese pedigrees showing Alzheimer's-type dementia and AD. Although the secretion of total Aβ was markedly reduced by this mutation, the variant Aβ was more resistant to proteolytic degradation. The mutant peptides showed the unique aggregation property of enhanced oligomerization but no fibrillization, and inhibited hippocampal long-term potentiation more potently than wild-type peptide in rats in vivo. Consistent with the nonfibrillogenic property of the variant Aβ, a very low amyloid signal was observed in the patient's brain on positron emission tomography using Pittsburgh compound-B.

Interpretation: The E693Δ mutation has been suggested as a cause of dementia because of enhanced formation of synaptotoxic Aβ oligomers. Our findings may provide genetic validation in humans for the emerging hypothesis that the synaptic and cognitive impairment in AD is primarily caused by soluble Aβ oligomers.

Ann Neurol 2008;63:377–387

Cerebral accumulation of the amyloid β (Aβ) peptide is a hallmark of Alzheimer's disease (AD). Based on studies in experimental models, soluble oligomers of Aβ, rather than amyloid fibrils, have been suggested as a means of initiation of the synaptic and cognitive dysfunction in AD.[1,2] Natural and synthetic Aβ oligomers have been shown to inhibit hippocampal long-term potentiation (LTP),[3–5] disrupt memory,[6,7] and decrease synaptic density.[8,9] However, there is no direct evidence in humans that this is a mechanism for the development of AD, and it is unknown whether Aβ oligomer formation is sufficient for disease development in the absence of fibril formation.

Genetic studies have demonstrated that many missense mutations in the amyloid precursor protein (APP) are associated with familial AD and cerebral amyloid angiopathy (CAA). These pathogenic mutations have been shown to influence Aβ metabolism by various means. For example, the Swedish double mutation (K670N/M671L)[10] adjacent to the β-cleavage site acts at the β-cleavage to increase production of total Aβ (both $Aβ_{1-40}$ and $Aβ_{1-42}$).[11] In contrast, mutations near the γ-cleavage site, such as the London (V717I, V717G),[12,13] Indiana (V717F),[14] and Florida (I716V)[15] mutations, cause the γ-cleavage to selectively increase the production of amyloidogenic $Aβ_{1-42}$.[16] Mutations within the Aβ sequence, including the Flemish (A692G),[17] Dutch (E693Q),[18] Italian (E693K),[19] Arctic (E693G),[20] and Iowa (D694N)[21] mutations, result in increased production of total Aβ[22]

From the [1]Department of Neuroscience, Osaka City University Graduate School of Medicine, Osaka; [2]Department of Physiology, Hyogo College of Medicine, Nishinomiya; [3]Department of Neurology, Osaka City University Graduate School of Medicine, Osaka; [4]Department of Bioinformatics, Brain Research Institute, Niigata University, Niigata; [5]Department of Neuropsychiatry, Imagawa Clinic; [6]Department of Physiology, Osaka City University Graduate School of Medicine, Osaka; and [7]Molecular Imaging Research Program, RIKEN, Kobe, Japan.

Received Aug 10, 2007, and in revised form Nov 16. Accepted for publication Nov 19, 2007.

Published online Feb 25, 2008, in Wiley InterScience (www.interscience.wiley.com). DOI: 10.1002/ana.21321

Address correspondence to Dr Mori, Department of Neuroscience, Osaka City University Graduate School of Medicine, 1-4-3 Asahimachi, Abeno-ku, Osaka 545-8585, Japan.
E-mail: mori@med.osaka-cu.ac.jp

Published by Wiley-Liss, Inc., through Wiley Subscription Services

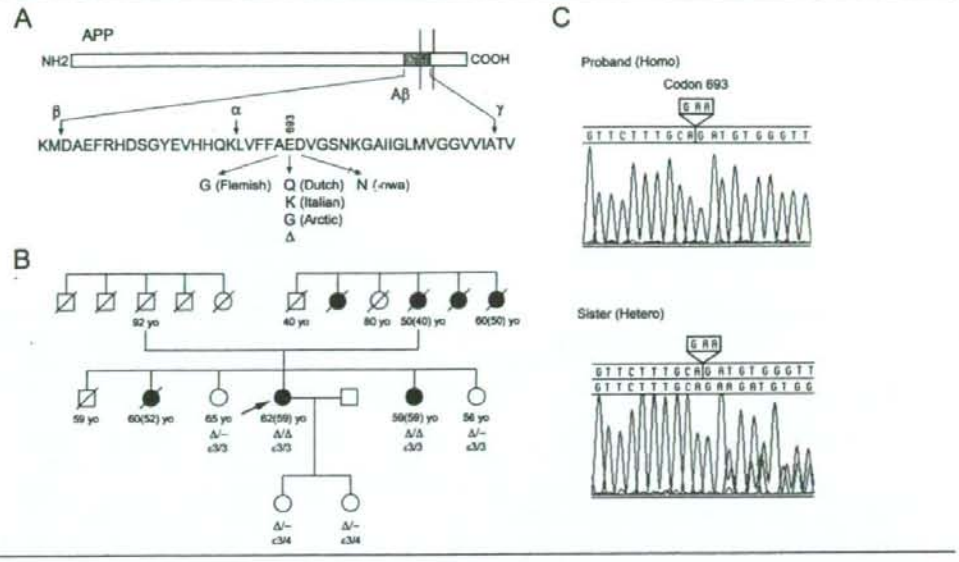

Fig 1. (A) Amyloid precursor protein (APP) mutations within the amyloid β (Aβ) sequence identified in certain families with Alzheimer's disease (AD) and cerebral amyloid angiopathy (CAA). The deletion (Δ) of E693 is the new mutation identified in this study. (B) Family tree of the pedigree with the E693Δ mutation. The proband is indicated with an arrow. *The ages of onset are shown in parentheses.* Solid symbols *denote affected;* open symbols *denote unaffected;* slashed symbols *denote deceased.* Δ = *deletion of* APP *codon 693 (GAA);* ○ = *female;* □ = *male. (C) DNA sequences of the proband (homozygote) and her unaffected sister (heterozygote).*

or enhanced propensity of Aβ to aggregate,[23,24] and in increased resistance of Aβ to proteolytic degradation.[25,26] All these alterations are presumed to lead to parenchymal or vascular amyloid formation, or both, as a consequence of Aβ accumulation in the brain.

In this study, we identified a novel *APP* mutation in Japanese pedigrees showing Alzheimer's-type dementia and AD. This mutation is the deletion of codon 693 (E693Δ) and is located within the Aβ sequence producing variant Aβ lacking glutamate at position 22 (E22Δ) (Fig 1A). To investigate the pathogenic roles of this mutation, we examined its effects on Aβ production, degradation, aggregation, and synaptotoxicity. Although the secretion of total Aβ was markedly reduced by this mutation, the variant Aβ was more resistant to degradation by two major Aβ-degrading enzymes, neprilysin[27] and insulin-degrading enzyme (IDE).[28] Synthetic Aβ E22Δ peptides showed a unique aggregation property of enhanced oligomerization but no fibrillization, and they inhibited hippocampal LTP more potently than wild-type peptide in vivo. Consistent with the nonfibrillogenic property of the variant Aβ, a very low amyloid signal was observed in the patient's brain on positron emission tomography (PET) using Pittsburgh compound-B (PIB).[29] These results suggest that the novel *APP* E693Δ mutation causes dementia by enhanced formation of synaptotoxic Aβ oligomers. Our findings may provide evidence in humans that synaptic and cognitive dysfunction in AD is caused by Aβ oligomers.

Subjects and Methods

Subjects

The proband was identified at the Osaka City University Hospital. Blood samples were obtained from her and her family members after an appropriate consultation in which they gave their informed consent to participate in this study. This study was approved by the institutional ethics committee of Osaka City University Graduate School of Medicine.

In addition to this family, we screened 5,310 Japanese people who were recruited for the Japanese Genetic Study Consortium for AD. They include patients with AD (n = 2,121), mild cognitive impairment (MCI; n = 128), dementia with Lewy bodies (n = 74), or other neurological diseases (n = 446) and control subjects (n = 2,541). Clinical AD cases met the criteria of the National Institute of Neurological and Communication Disorders-Alzheimer's Disease and Related Disorders Association. Informed consent was obtained from all control subjects and appropriate proxies for patients. This study was approved by the institutional review board of Niigata University and by all participating hospitals.

Genetic Analysis

Exons 16 and 17 of *APP* and all exons of two presenilin genes (*PSEN1* and *PSEN2*) were amplified by polymerase

Table 1. **Fifteen Polymorphic Microsatellite Markers around the APP Gene**

No.	Marker	cM	Mb
1	D21S1884	14.20	21.549
2	D21S1914	19.39	24.544
3	D21S1907	20.45	25.489
4	D21S265	20.45	25.841
5	D21S1268		26.114
6	Mutation		26.186
7	D21S1253	20.45	26.356
8	D21S1443		26.445
9	D21S1896	21.88	26.746
10	D21S260	22.59	26.893
11	D21S269	22.59	26.923
12	D21S1442	24.73	27.740
13	D21S1258	24.73	27.742
14	D21S1916	25.26	27.903
15	D21S1915	25.80	28.042
16	D21S263	27.40	31.144

Two of the markers (D21S1253 and D21S1443) are included in the *APP* gene (at positions 26174732-26465003). Marker references, genetic distance in centimorgans (cM) (Marshfield map), and physical positions in Mb on chromosome 21 are shown.

chain reaction (PCR) from genomic DNA from the proband and her family members, and analyzed by direct DNA sequencing. Apolipoprotein E genotype was determined as described previously.[30]

Genomic DNA from 5,310 Japanese people was anonymously analyzed for the newly identified E693Δ mutation using an ABI 7900HT Fast Realtime PCR System (Applied Biosystems, Tokyo, Japan) and TaqMan SNP Genotyping Assays (Applied Biosystems). We designed two fluorescently labeled TaqMan probes to distinguish wild-type and mutant alleles: VIC-labeled 5−-AACCCACATCTTCTG-3− for wild-type allele and 6-FAM-labeled 5−-TTTGAACCCACATCTG-3− for the mutant allele. Samples found to be positive for the mutation in this assay were further examined by DNA sequencing. To study the genetic relation among the mutation carriers, we performed haplotype analysis of their genomic DNA around the *APP* gene. We used 15 polymorphic microsatellite markers near the mutation (summarized in Table 1). The marker information and sequences of PCR primers were from a public Web site (National Center for Biotechnology Information, Build 36; http://www.ncbi.nlm.nih.gov). Alleles of each marker were determined by the length of PCR products with fluorescently labeled primers using an ABI 3730 DNA analyzer and GeneMapper 3.0 software (Applied Biosystems). Haplotypes of the carriers were constructed manually.

Analysis of Cerebrospinal Fluid

Cerebrospinal fluid (CSF) samples (0.5–1.5 ml) were obtained from the proband and patients with AD (n = 5) or other neurological disorders (n = 12) after an appropriate consultation at the Osaka City University Hospital. Aβ concentrations in the samples were measured by enzyme-linked immunosorbent assay (ELISA), as described later. For detection of Aβ oligomers, each CSF sample was adjusted to 1ml with TS (100mM tris[hydroxymethyl]aminomethane-HCl, pH 7.6, 150mM NaCl) and supplemented with a protease-inhibitor cocktail (P8340; Sigma, St. Louis, MO). The Aβ in the samples was then immunoprecipitated with 10μg anti-Aβ 6E10 antibody (Signet Laboratories, Dedham, MA) and analyzed by Western blotting, as described later. Aβ monomers, dimers, and trimers were quantified using an LAS-3000 luminescent image analyzer (Fujifilm, Tokyo, Japan), as described previously.[31]

Amyloid Imaging

Amyloid imaging of the patient's brain with a PET tracer [^{11}C]PIB was performed using a PET scanner Eminence-B (Shimadzu, Kyoto, Japan), which was composed of 352 detector blocks, each with a 6 × 8 array of 3.5 × 6.25 × 30mm^3 bismuth germinate oxyorthosilicate crystals, arranged as 32 crystal rings with a 208mm axial field of view. Transmission scans were performed before PIB administration for 5 minutes in singles mode with a ^{137}Cs point source to obtain attenuation correction data. Emission data were acquired over 60 minutes (29 frames: 6 × 30, 12 × 60, 5 × 180, 6 × 300 seconds). Images were reconstructed with segmented attenuation correction, using Fourier rebinning followed by two-dimensional filtered back-projection applying Ramp filter cutoff at Nyquist frequency. A three-dimensional Gaussian filter with a kernel full-width at half maximum of 5mm was applied to the images as a post filter. All subjects received an intravenous bolus injection of 150 to 300MBq PIB with a high specific activity (average 20–30GBq/μmol). PIB retention data were given as standard uptake values, as described previously.[29]

Amyloid Precursor Protein Constructs

Wild-type human APP_{695} (APP_{WT}) complementary DNA was amplified by PCR from pooled human complementary DNA and cloned into a pCI mammalian expression vector (Promega, Tokyo, Japan). Mutant APP complementary DNA with the E693Δ, Swedish (K670N/M671L), and London (V717I) mutations ($APP_{E693\Delta}$, APP_{SW}, APP_{LD}, respectively) were prepared by site-directed mutagenesis.

Mass Spectrometry

Human embryonic kidney 293 (HEK293) cells were transfected with APP constructs and cultured in serum-free medium for 3 days. Aβ in the conditioned media was immunoprecipitated with an antibody to the N-terminal region of Aβ (β001)[32] or an antibody specific to the C terminus of AβX-40 (Ter40)[33] and subjected to matrix-assisted laser desorption ionization-time of flight mass spectrometry using an AXIMA-CFR matrix-assisted laser desorption ionization-time of flight mass spectrometric analyzer (Shimadzu).

Peptides

Based on the results of mass spectrometry, the mutant $A\beta_{1-42}$ E22Δ and $A\beta_{1-40}$ E22Δ peptides were synthesized (American Peptide Company, Sunnyvale, CA). The molecular weight and amino acid composition of the peptides were confirmed by electrospray mass-spectral analysis and amino acid analysis, respectively. The purity of the two peptides was 91.0% and 95.0%, respectively, which was determined by reverse-phase high-pressure liquid chromatography. Control wild-type $A\beta_{1-42}$ and $A\beta_{1-40}$ peptides were purchased from the American Peptide Company and from the Peptide Institute (Osaka, Japan).

Enzyme-Linked Immunosorbent Assay

HEK293 cells were transfected with APP constructs and cultured in serum-free medium for 3 days. Aβ concentrations in the conditioned media were measured by ELISA using Human Amyloid β (1-42) (N) and (1-40) (N) kits (IBL, Gunma, Japan). To make standard curves, we serially diluted synthetic Aβ peptides dissolved in dimethylsulfoxide (DMSO) in standard dilution buffer supplied in the kits. For measurement of the mutant Aβ, synthetic Aβ E22Δ peptides were used as standards. The expression level of the APP in each transfectant was evaluated by Western blotting with an antibody to the C terminus of APP (C40).[34]

Degradation Assay

Human neprilysin was prepared as described previously.[31] For human IDE, the cytosol fraction of untransfected HEK293 cells, which contains endogenous IDE, was prepared as a crude enzyme preparation. A degradation assay with neprilysin was performed as described previously.[31] With IDE, synthetic $A\beta_{1-40}$ peptides were incubated with the enzyme in the presence or absence of 100μM insulin at 37°C for 4 hours in 100mM HEPES (pH 7.4) solution. The reaction was stopped by adding sodium dodecyl sulfate sample buffer to the mixture and boiling. Residual intact Aβ was detected by Western blotting with 6E10 and quantified using an LAS-3000 luminescent image analyzer.

Aggregation Studies

Synthetic $A\beta_{1-42}$ and $A\beta_{1-40}$ peptides were initially dissolved to 0.1mM in the α-helix–promoting solvent hexafluoroisopropanol (Sigma), and the solvent was evaporated under vacuum. The dried peptides were resuspended to 1mM in 0.1% NH_4OH and dispensed, in quadruplicate, into tubes containing phosphate-buffered saline (PBS) to make a peptide concentration of 100μM. The peptide solutions were incubated at 37°C for 7 days; aliquots were taken every 24 hours to monitor peptide aggregation by thioflavin T fluorescence assay.[35] For Western blotting, the aliquots were diluted in sodium dodecyl sulfate sample buffer, boiled, and subjected to Western blotting with 6E10 and β001. Samples that had been incubated for 7 days were also subjected to electron microscopy to examine fibril formation. In some experiments, hexafluoroisopropanol-treated, dried $A\beta_{1-42}$ peptides were dissolved in DMSO and diluted in PBS to make peptide concentrations of 100, 10, and 1μM in 10% DMSO/PBS, and subjected to Western blotting soon after peptide solubilization.

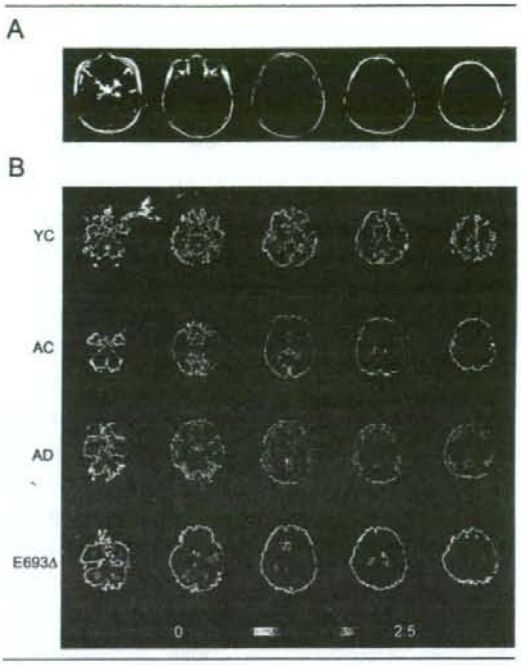

Fig 2. (A) Magnetic resonance imaging of the proband's brain at 62 years old. (B) Amyloid imaging of the proband's brain with [^{11}C] Pittsburgh compound-B (PIB). PIB standardized uptake value images summed over 40 to 60 minutes are shown. YC = young control (29-year-old man); AC = aged control (81-year-old woman); AD = Alzheimer's disease (71-year-old woman); E693Δ = proband (62-year-old woman).

In Vivo Electrophysiology

Electrophysiological experiments were performed on male adult Wistar rats, essentially as described previously.[3] Synthetic $A\beta_{1-42}$ peptides were dissolved to 50ng/μl in hexafluoroisopropanol, dried, and resuspended in the same volume of 0.1% NH_4OH. The peptide solutions were dispensed into tubes and frozen at −80°C until use. For microinjection, the frozen solutions were diluted with PBS to make a peptide concentration of 5ng/μl and kept on ice to avoid peptide aggregation. Two microliters (10ng Aβ peptide) of the samples or PBS alone was injected into the rat cerebral ventricle over 30 seconds through an implanted cannula 10 minutes before the LTP induction. LTP was induced using theta burst stimulation consisting of 4 trains of 10 bursts of 10 pulses (0.1-millisecond duration, 200Hz), with an interburst interval of 200 milliseconds and an intertrain interval of 30 seconds. The slopes of two consecutive field excitatory postsynaptic potentials were averaged every minute and expressed as a percentage of the baseline slope.

Results

Clinical Description of the Proband

The proband was a 62-year-old Japanese woman. Her pedigree, which originated from an island in the west-

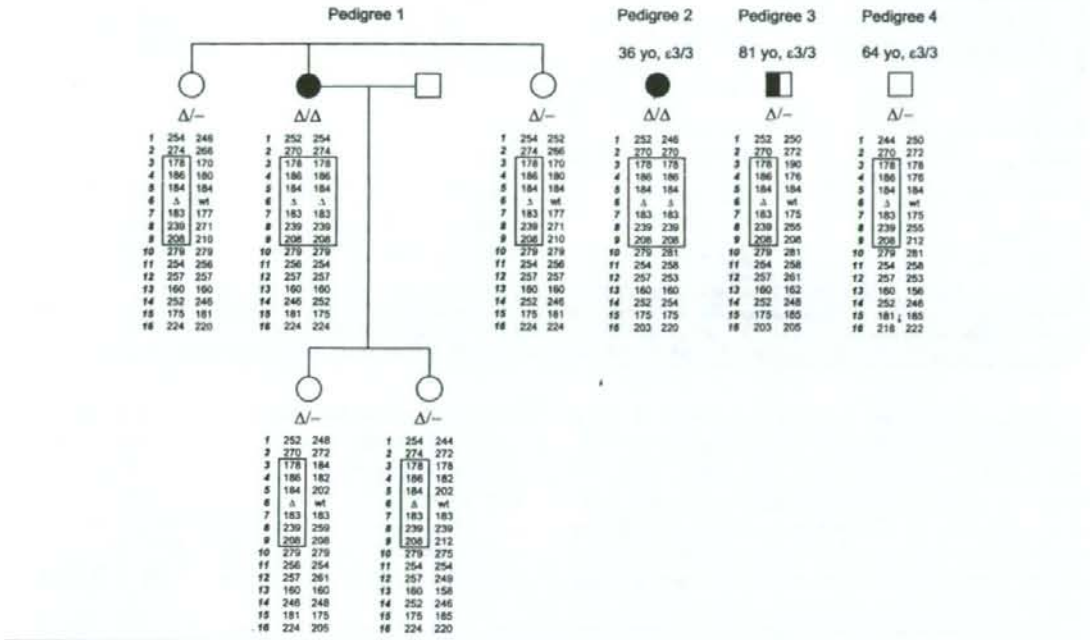

Fig 3. Haplotype analysis of four pedigrees with the E693Δ mutation around the amyloid precursor protein (APP) *gene.* Solid symbols *denote Alzheimer's disease (AD);* half-solid symbol *denotes mild cognitive impairment (MCI);* open symbols *denote unaffected.* Δ = *deletion of* APP *codon 693 (GAA). Fifteen polymorphic microsatellite markers were examined to investigate the relations between the pedigrees, and their alleles are shown. The boxed alleles (178-186-184-Δ-183-239-208) ranging from positions 25488483 to 26746210 on chromosome 21 represent the common haplotype among the mutation carriers.*

ern area of Japan, is highly consanguineous and includes a history of hereditary dementia (see Fig 1B). She had no history or symptoms of other neurological disorders but noticed memory disturbance at 55 years of age and sought treatment at the hospital at 57 years. Her Mini-Mental State Examination (MMSE) score was normal, and she was diagnosed as having MCI. Magnetic resonance imaging and PET showed neither cortical atrophy nor abnormal glucose metabolism, whereas single-photon emission computed tomography demonstrated mild hypoperfusion in the temporal lobes. An electroencephalogram showed bilateral, intermittent, generalized slow theta activity. At 59 years old, her MMSE score dropped to 22/30, and according to the *Diagnostic and Statistical Manual of Mental Disorders,* Third Edition Revised and the criteria of the National Institute of Neurological and Communication Disorders-Alzheimer's Disease and Related Disorders Association, she was diagnosed as having AD. At 61 years old, her symptoms worsened and her MMSE score had decreased to 18. She exhibited cerebellar ataxia, gait disturbance, ideomotor apraxia, and pyramidal signs such as abnormal Babinski's and Chaddock's reflexes. Despite the severe dementia (MMSE score of 5) at 62 years old, only mild parietal lobe atrophy was observed on magnetic resonance imaging (Fig 2A). Based on this clinical complexity, we diagnosed this patient as having "Alzheimer's-type dementia" rather than AD.

Identification of a Novel APP Mutation

From the proband and her family members, we identified a novel mutation in *APP* exon 17 with no mutations in *PSEN1* or *PSEN2.* This *APP* mutation is the deletion of codon 693 (GAA) encoding glutamate-22 in the Aβ sequence. The proband had the homozygous deletion, whereas her unaffected older and younger sisters (65 and 56 years, respectively) showed only the heterozygous deletion (see Fig 1C). Recently, another of her sisters (59 years old) came to show cognitive decline, and we found that she also had the homozygous deletion (see Fig 1B). The apolipoprotein E4 genotype was not associated with this familial case (see Fig 1B). This E693Δ mutation is the first deletion-type mutation discovered in *APP.*

To investigate the association of this mutation with AD or Alzheimer's-type dementia, we screened 5,310 Japanese people with or without AD. The same ho-

Table 2. Production of Amyloid β E22Δ from Cells

APP Constructs	$A\beta_{1-42}$ (pg/ml)	$A\beta_{1-40}$ (pg/ml)	$A\beta_{1-42/1-40}$ ratio (%)
APP_{WT}	88 ± 7	797 ± 86	11.0 ± 0.5
$APP_{E693\Delta}$	54 ± 6	495 ± 18	11.0 ± 1.5
APP_{SW}	1,380 ± 47	18,653 ± 1759	7.4 ± 0.5
$APP_{SW/E693\Delta}$	782 ± 90	11,882 ± 935	6.6 ± 0.5
$APP_{SW/LD}$	3,218 ± 94	16,475 ± 681	19.6 ± 0.9
$APP_{SW/E693\Delta/LD}$	1,872 ± 144	8,974 ± 981	21.0 ± 1.7

Concentrations of $A\beta_{1-42}$ and $A\beta_{1-40}$ in conditioned media from human embryonic kidney 293 (HEK293) cells transfected with amyloid precursor protein (APP) constructs were determined by enzyme-linked immunosorbent assay. No difference in APP expression levels was observed among transfectants. Data are means ± standard deviation for quadruplicate transfections.
Aβ = amyloid β; WT = wild type; SW = Swedish (K670N/M671L) mutation; LD = London (V717I) mutation.

mozygous deletion was detected in a patient showing AD (36 years old, ε3/3), and the heterozygous deletion was found in two individuals, one having MCI (81 years old, ε3/3) and the other being healthy (64 years old, ε3/3) (Fig 3). This newly identified homozygote with AD had been recorded to already show cognitive decline with a MMSE score of 15 at his first medical examination without exhibiting any other symptoms, such as cerebellar ataxia, gait disturbance, ideomotor apraxia, and pyramidal signs. Thus, it is likely that the atypical symptoms observed in the proband are not part of an obligatory E693Δ mutation phenotype.

We then examined 15 polymorphic microsatellite markers around the *APP* gene (see Table 1) of the mu-

Table 3. Amyloid β Levels in Human Cerebrospinal Fluid

Patient No.	Diagnosis	Age (yr)/Sex	$A\beta_{1-42}$ (pg/ml)	$A\beta_{1-40}$ (pg/ml)	$A\beta_{1-42/1-40}$ Ratio (%)
1	MS	55/F	745	3,193	23.3
2	MS	71/F	792	2,862	27.7
3	CIPD	30/M	503	1,809	27.8
4	MS	24/F	344	1,033	33.3
5	Polyneuropathy	64/F	923	3,382	27.3
6	MS	32/F	673	2,165	31.1
7	Polyneuropathy	38/M	989	3,229	30.6
8	SLE	25/F	289	949	30.4
9	Parkinson's syndrome	68/M	339	916	37.1
10	MSA	64/M	653	2,165	30.2
11	Myelitis	30/M	701	2,525	27.8
12	Angitis	71/M	504	1,817	27.8
13	AD	64/F	258	1,628	15.9
14	AD	68/M	360	3,041	11.8
15	AD	73/F	687	5,055	13.6
16	AD	72/F	381	2,008	19.0
17	AD/SP[a]	27/M	113	1,109	10.2
18	Alzheimer's-type dementia	59/F	22	390	5.7

Concentrations of $A\beta_{1-42}$ and $A\beta_{1-40}$ in cerebrospinal fluid (CSF) samples were determined by enzyme-linked immunosorbent assay (ELISA). The proband with the E693Δ mutation is shown as #18.
[a]This patient has a *PSEN1* mutation (L85P).[36]
Aβ = amyloid β; MS = multiple sclerosis; CIPD = chronic inflammatory demyelinating polyneuropathy; SLE = systemic lupus erythematosus; MSA = multiple system atrophy; AD = Alzheimer's disease; AD/SP = AD with spastic paraparesis.

tation carriers to determine their genetic relation. The results demonstrated that they do not belong to the same pedigree, although they may have a common ancestor (see Fig 3). It is noteworthy that three homozygotes in two different pedigrees were all affected with dementia, suggesting that this mutation, particularly its homozygous occurrence, is a cause of the disease.

Amyloid β Species Produced from the Mutant Amyloid Precursor Protein

To identify Aβ species produced from the mutant APP, we examined the molecular mass of Aβ secreted from HEK293 cells transfected with an $APP_{E693\Delta}$ construct. The resultant Aβ was found to start and end at normal positions but lack a glutamate, as predicted (data not shown). Based on this information, we synthesized Aβ peptides 1 to 40 and 1 to 42 with the E22Δ mutation and performed the experiments described in the following sections.

Production of the Mutant Amyloid β

The effect of the E693Δ mutation on Aβ production was assessed in HEK293 cells transfected with APP constructs. We confirmed no difference in APP expression levels among transfectants. The concentrations of $Aβ_{1-42}$ and $Aβ_{1-40}$ in conditioned media were measured by ELISA with antibodies specific to the N and C terminus of each peptide. Compared with APP_{WT}, the mutant $APP_{E693\Delta}$ produced low levels of $Aβ_{1-42}$ and $Aβ_{1-40}$ with an unaffected ratio of $Aβ_{1-42/1-40}$ (Table 2). This effect was observed even in the presence of the Swedish and London mutations (see Table 2).

The reduced secretion of the mutant $Aβ_{1-42}$ and $Aβ_{1-40}$ was confirmed in the CSF from the proband (Table 3). The ratio of $Aβ_{1-42/1-40}$ in the proband's CSF was markedly reduced, suggesting enhanced cerebral accumulation of the mutant $Aβ_{1-42}$.

Degradation of the Mutant Amyloid β

$Aβ_{1-40}$ peptides with a missense mutation at positions 21, 22, or 23 have been shown to be more resistant than wild-type peptide to degradation by neprilysin[25] and IDE.[26] Thus, we examined the effect of the E22Δ mutation on Aβ degradation. Synthetic $Aβ_{1-40}$ peptides were incubated with each enzyme preparation, and residual intact peptides were detected by Western blotting with 6E10. The mutant E22Δ peptide was shown to be more resistant than wild-type peptide to degradation by both neprilysin and IDE (Fig 4).

Aggregation of the Mutant Amyloid β

Next, we examined the effect of the E22Δ mutation on Aβ aggregation. In the thioflavin T fluorescence assay, which measures peptide fibrillization,[35] wild-type $Aβ_{1-42}$ and $Aβ_{1-40}$ peptides (100μM) produced a rapid increase in fluorescence, whereas the mutant peptides

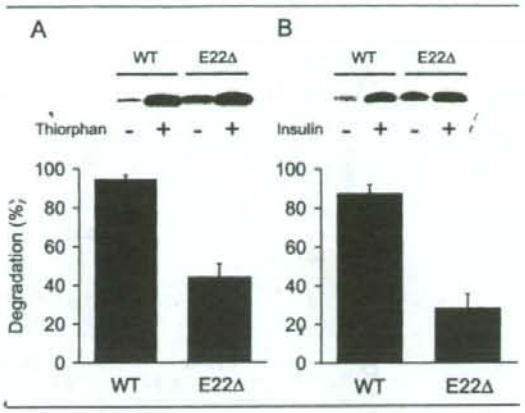

Fig 4. Degradation of amyloid β (Aβ) E22Δ peptide by neprilysin and insulin-degrading enzyme (IDE). (A) Synthetic $Aβ_{1-40}$ peptides (1μM) were incubated with purified recombinant neprilysin in the presence or absence of its specific inhibitor, thiorphan (50μM). Residual intact peptide was detected by Western blotting with 6E10. (B) $Aβ_{1-40}$ peptides were incubated with a crude IDE preparation in the presence or absence of its physiological substrate, insulin (100μM), which was expected to act as a competitive inhibitor. WT = wild type.

exhibited no significant increase (Fig 5A). It was shown using Western blotting that wild-type $Aβ_{1-42}$ and $Aβ_{1-40}$ peptides undergo a time-dependent decrease of monomers, reflecting their aggregation into fibrils, whereas monomers of the mutant peptides decrease modestly or not at all (see Fig 5B). Moreover, the mutant peptides displayed striking formation of sodium dodecyl sulfate–stable oligomers (dimers, trimers, and tetramers) immediately after their solubilization, and these declined little, if at all, over the 7-day incubation. This rapid oligomerization by the mutant peptides was observed even at lower peptide concentrations (10 and 1μM; see Fig 5C). Abundant dimers, trimers, and tetramers were detected in the mutant peptide at all concentrations we tested, whereas wild-type peptide formed only a small number of oligomers at greater concentrations. Electron microscopy showed that wild-type $Aβ_{1-42}$ peptide formed abundant fibrils, whereas essentially no fibrillization was observed with the mutant peptide (see Fig 5D). Taken together, these various assays show that the E22Δ peptides rapidly form stable low-n oligomers but undergo no detectable transformation into fibrils.

Presence of Amyloid β Oligomers in the Patient's Cerebrospinal Fluid

To confirm the enhanced oligomerization of the mutant Aβ, we examined CSF samples from the proband and patients with neurological disorders including AD. All samples tested displayed Aβ dimers and trimers, as

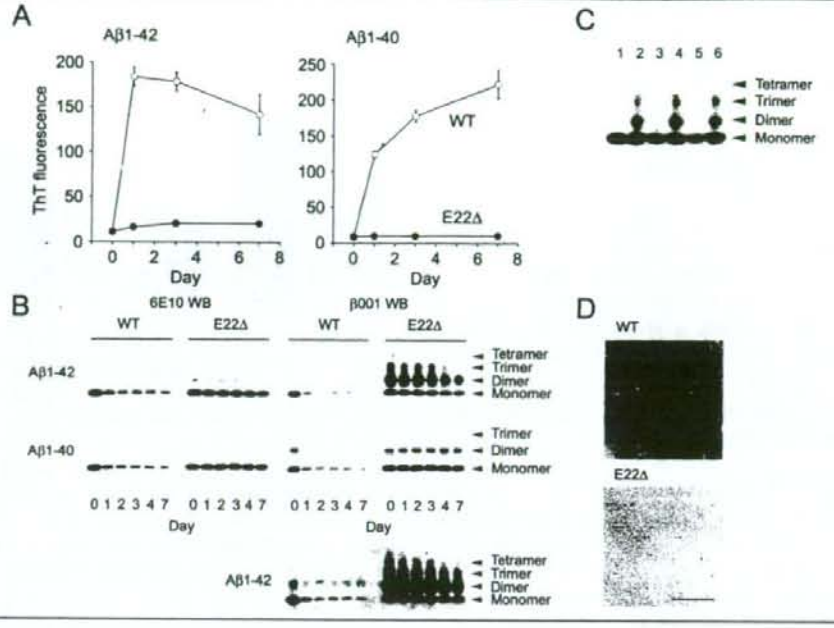

Fig 5. Aggregation of amyloid β (Aβ) peptides with or without the E22Δ mutation. Synthetic $Aβ_{1-42}$ and $Aβ_{1-40}$ peptides were incubated at 100μM in phosphate-buffered saline (PBS) at 37°C for 7 days (A, B, D). (A) Aggregation into fibrils was monitored by thioflavin T fluorescence assay. Each point *represents the mean ± standard deviation for quadruplicate determinations. (B) Oligomerization was examined by Western blotting with 6E10 and βΟΟ1. It was shown that Aβ monomers were stained well with 6E10 rather than with βΟΟ1, whereas Aβ oligomers were intensely stained with βΟΟ1 but not so much with 6E10. (B, bottom right) Longer exposure of the $Aβ_{1-42}$ blot stained with βΟΟ1. (C) $Aβ_{1-42}$ peptides were dissolved at 100, 10, and 1μM in 10% dimethylsulfoxide/PBS. Oligomerization was examined soon after peptide solubilization by Western blotting with the mixture of 6E10 and βΟΟ1. Lanes 1, 3, 5: wild-type (WT) peptide; lanes 2, 4, 6: mutant peptide; lanes 1, 2: 100μM; lanes 3, 4: 10μM; lanes 5, 6: 1μM. Samples were adjusted so that they contained the same peptide amount when they were loaded on the gel. (D) After a 7-day incubation, $Aβ_{1-42}$ peptides were examined for fibrils by electron microscopy. Scale bar = 100nm.*

well as monomers, in our immunoprecipitation/Western blotting analysis (Fig 6A). Densitometric analysis demonstrated that the proband's CSF showed a greater ratio of oligomers/monomers (about 1.5) than other samples (mean value of about 0.7), although one sample displayed a similar level of Aβ oligomerization to the proband's CSF (see Fig 6B).

Little Amyloid Deposition in the Patient's Brain

The nonfibrillogenic property of the E22Δ mutant Aβ was predictive of a lack of deposition of fibrillar amyloid in the patient's brain. To assess this possibility in a family with no brain autopsies conducted to date, we performed PET amyloid imaging of the proband with [^{11}C]PIB.[29] Slight but significant PIB retention signals were observed in the temporal, parietal, and occipital lobes and in the cerebellum, but not in the frontal lobe, a signal that is far less than that observed in typical idiopathic AD brains (see Fig 2B). Thus, the lower ability to form amyloid fibrils of the mutant Aβ was observed both in vitro and in the human brain in vivo.

Synaptotoxicity of the Mutant Amyloid β

Recent reports of Aβ oligomer-induced synaptic dysfunction[3–5] led us to examine the effects of the mutant versus wild-type Aβ on synaptic plasticity in vivo. Before the injection of Aβ into the rat cerebral ventricle, we examined the aliquots of the injection samples to confirm that the mutant peptide formed more abundant oligomers than wild-type peptide (Fig 7A). The ratios of oligomers (dimers, trimers, and tetramers) to monomers of the mutant and wild-type peptides were about 1.1 and 0.4, respectively. As shown previously,[3] wild-type peptide caused a significant inhibition of LTP in rats in vivo (see Fig 7B). Notably, the mutant peptide showed a much stronger inhibition than wild-type peptide. The observed results appear to reflect the greater ability of the mutant peptide to form stable oligomers, which are known to abrogate hippocampal

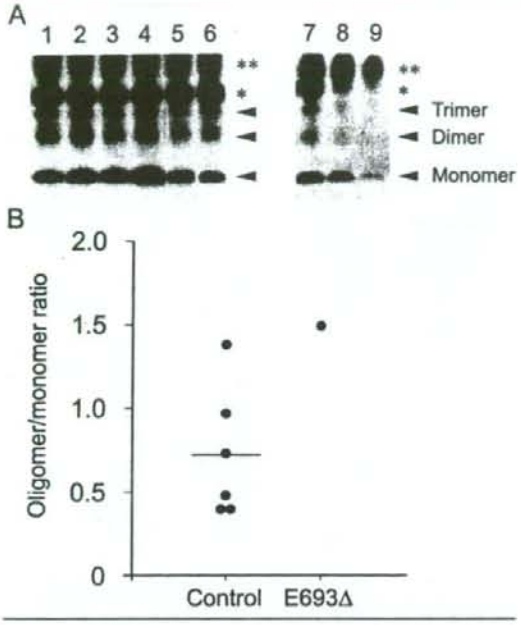

Fig 6. The presence of amyloid β (Aβ) oligomers in the proband's cerebrospinal fluid (CSF). The volume of each CSF sample (lanes 1–5: 0.5ml; lane 6: 1.0ml; lanes 7–9: 0.4, 0.2, and 0.1ml) was adjusted to 1.0ml with TS. Aβ in the samples was then immunoprecipitated with 10μg 6E10 and analyzed by Western blotting with the mixture of 6E10 and β001. (A) Lane 1: Patient 4; lane 2: Patient 12; lane 3: Patient 13; lane 4: Patient 14; lane 5: Patient 17; lane 6: Patient 18 (the proband with E693Δ mutation); and lanes 7–9: Patient 9 in Table 3. Asterisks *indicate nonspecific bands probably derived from CSF because these bands attenuated as CSF input was decreased (lanes 7–9). (B) The ratio of oligomers (dimers and trimers) to monomers in each sample was plotted.*

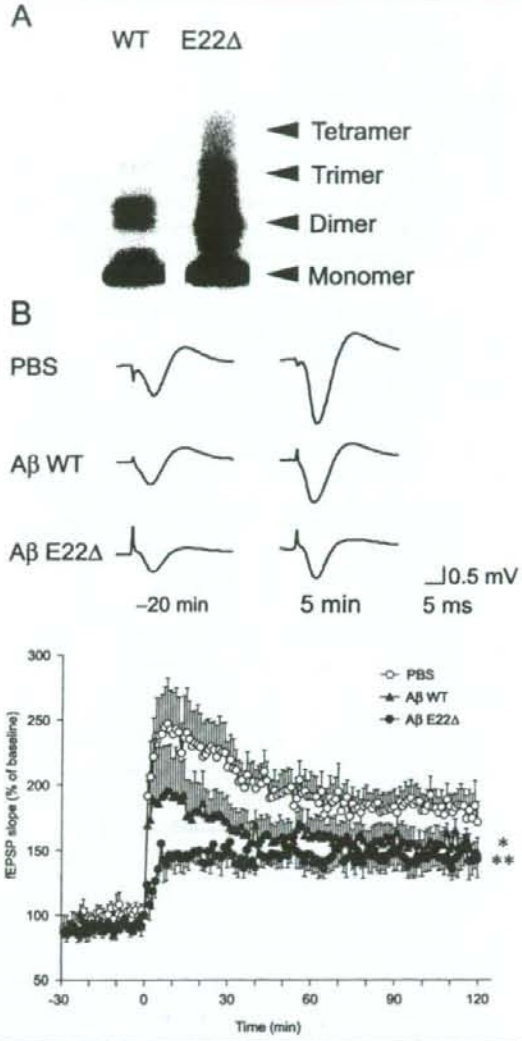

Fig 7. In vivo synaptotoxicity of $A\beta_{1-42}$ E22Δ peptide in rats. (A) Aβ oligomerization in the injection samples was confirmed by Western blotting with β001. (B) Long-term potentiation (LTP) in the hippocampal CA1 region was induced by delivering theta burst stimulation (TBS) to the Schaffer collateral/commissural pathway. Aβ peptides (10ng in 2μl phosphate-buffered saline [PBS]) were injected into the lateral ventricle 10 minutes before TBS. Typical field excitatory postsynaptic potentials at −20 and 5 minutes after TBS are shown above. Each point on the graph represents the mean ± standard error of the mean. n = 4 for PBS (open circles) *and wild-type (WT)* $A\beta_{1-42}$ (triangles); *n = 5 for* $A\beta_{1-42}$ *E22Δ* (solid circles). *$^{*}p = 0.0497$ versus PBS; $^{**}p < 0.0001$ versus PBS; $p < 0.0001$ versus wild-type, when field excitatory postsynaptic potential (fEPSP) slopes were compared 1 to 120 minutes after TBS. Comparisons of the means between the three groups were performed using an analysis of variance followed by Fisher's PLSD test.*

LTP in vivo and in vitro in the absence of Aβ monomers, protofibrils, and fibrils.[3,4]

Discussion

Missense mutations in *APP* linked to familial AD and CAA are thought to cause disease by affecting Aβ production, degradation, and aggregation. This E693Δ mutation was also found to influence Aβ metabolism. However, its effects appear to be unique compared with other *APP* mutations.

The E693Δ mutation significantly reduced total Aβ secretion and did not affect the $A\beta_{1-42/1-40}$ ratio. This reduction might be caused by altered APP processing, that is, reduced β- or γ-cleavage, or by disturbed secretion of Aβ generated intracellularly. The mechanisms underlying this reduction are yet to be studied. Furthermore, the mutant Aβ was more resistant than

wild-type Aβ to degradation by two major Aβ-degrading enzymes, neprilysin and IDE. This proteolytic resistance may result in a prolonged half-life of the mutant Aβ in the brain, and this may, in part, counteract the reduced secretion. Moreover, the mutant Aβ did not exhibit fibrillization but did enhance oligomerization. Consistent with this observation, PIB-PET amyloid imaging demonstrated little deposition of fibrillar amyloid in the patient's brain. These results suggest that the E693Δ mutation causes disease by the mechanism other than enhancing amyloid fibril formation.

Recent evidence suggests that soluble oligomers of Aβ, rather than amyloid fibrils, play a crucial role in synaptic and cognitive dysfunction in the early stages of AD.[1,2] The E693Δ mutation promoted a high level of Aβ oligomerization, and the mutant Aβ peptide caused more potent inhibition of hippocampal LTP than wild-type peptide in vivo. This toxic effect may be extended by increased resistance of the mutant Aβ to proteolytic degradation. Thus, the E693Δ mutation has been suggested to cause dementia by enhanced formation of synaptotoxic Aβ oligomers.

Regarding the results of PIB-PET analysis, it should be kept in mind that the slight but significant PIB retention signals observed in the patient's brain may indicate, in fact, the presence of certain amounts of amyloid fibrils, and that their distribution was rather similar to that observed in CAA.[36] Furthermore, we cannot exclude the possibility that the mutant Aβ was not a good substrate for PIB. It may be that, at least in the proband, the E693Δ mutation caused CAA and dementia, although our in vitro aggregation studies appeared not to support this idea.

Our finding that homozygotes, but not heterozygotes, showed AD or Alzheimer's-type dementia appears to indicate that the E693Δ mutation represents the first recessive mutation linked to the disease. However, it is possible that this may reflect incomplete penetrance of this mutation. The fact that one of the heterozygotes had MCI, a harbinger of AD, suggests that this mutation may act in a dose-dependent manner, similar to apolipoprotein E4.[37] In either case, this is different from other known *APP* mutations that have been shown to cause disease in a fully penetrant fashion. This issue requires further genetic study.

In conclusion, the novel *APP* E693Δ mutation identified in familial Alzheimer's-type dementia and AD has been suggested to cause disease by enhanced Aβ oligomerization. Our findings may provide genetic validation in humans for the emerging hypothesis that synaptic and cognitive impairment in AD is much more closely linked to Aβ oligomer formation than to amyloid fibril formation. Further investigation is required with prospective brain autopsy and/or animal models harboring this mutation to determine its exact pathology.

This study was supported by MEXT of Japan (grants-in-aid for Scientific Research on Priority Areas-Research on Pathomechanisms of Brain Disorders 18023033 and 17300114 [H. Mori]).

We thank Dr Y. Ihara for his continuous encouragement and helpful discussion throughout this study.

References

1. Selkoe DJ. Alzheimer's disease is a synaptic failure. Science 2002;298:789–791.
2. Klein WL, Krafft GA, Finch CE. Targeting small Aβ oligomers: the solution to an Alzheimer's disease conundrum? Trends Neurosci 2001;24:219–224.
3. Walsh DM, Klyubin I, Fadeeva JV, et al. Naturally secreted oligomers of amyloid β protein potently inhibit hippocampal long-term potentiation *in vivo*. Nature 2002;416:535–539.
4. Townsend M, Shankar GM, Mehta T, et al. Effects of secreted oligomers of amyloid β-protein on hippocampal synaptic plasticity: a potent role for trimers. J Physiol 2006;572:477–492.
5. Lambert MP, Barlow AK, Chromy BA, et al. Diffusible, nonfibrillar ligands derived from $A\beta_{1-42}$ are potent central nervous system neurotoxins. Proc Natl Acad Sci USA 1998;95:6448–6453.
6. Cleary JP, Walsh DM, Hofmeister JJ, et al. Natural oligomers of the amyloid-β protein specifically disrupt cognitive function. Nat Neurosci 2005;8:79–84.
7. Lesné S, Koh MT, Kotilinek L, et al. A specific amyloid-β protein assembly in the brain impairs memory. Nature 2006;440:352–357.
8. Shankar GM, Bloodgood BL, Townsend M, et al. Natural oligomers of the Alzheimer amyloid-β protein induce reversible synapse loss by modulating an NMDA-type glutamate receptor-dependent signaling pathway. J Neurosci 2007;27:2866–2875.
9. Lacor PN, Buniel MC, Furlow PW, et al. Aβ oligomer-induced aberrations in synapse composition, shape, and density provide a molecular basis for loss of connectivity in Alzheimer's disease. J Neurosci 2007;27:796–807.
10. Mullan M, Crawford F, Axelman K, et al. A pathogenic mutation for probable Alzheimer's disease in the APP gene at the N-terminus of β-amyloid. Nat Genet 1992;1:345–347.
11. Citron M, Oltersdorf T, Haass C, et al. Mutation of the β-amyloid precursor protein in familial Alzheimer's disease increases β-protein production. Nature 1992;360:672–674.
12. Goate A, Chartier-Harlin M-C, Mullan M, et al. Segregation of a missense mutation in the amyloid precursor protein gene with familial Alzheimer's disease. Nature 1991;349:704–706.
13. Chartier-Harlin M-C, Crawford F, Houlden H, et al. Early-onset Alzheimer's disease caused by mutations at codon 717 of the β-amyloid precursor protein gene. Nature 1991;353:844–846.
14. Murrell J, Farlow M, Ghetti B, Benson MD. A mutation in the amyloid precursor protein associated with hereditary Alzheimer's disease. Science 1991;254:97–99.
15. Eckman CB, Mehta ND, Crook R, et al. A new pathogenic mutation in the APP gene (I716V) increases the relative proportion of Aβ42(43). Hum Mol Genet 1997;6:2087–2089.
16. Suzuki N, Cheung TT, Cai X-D, et al. An increased percentage of long amyloid β protein secreted by familial amyloid β protein precursor (βAPP_{717}) mutants. Science 1994;264:1336–1340.
17. Hendriks L, van Duijn CM, Cras P, et al. Presenile dementia and cerebral haemorrhage linked to a mutation at codon 692 of the β-amyloid precursor protein gene. Nat Genet 1992;1:218–221.